Spectrochimica Acta Part A 94 (2012) 243–255

Contents lists available at SciVerse ScienceDirect

Spectrochimica Acta Part A: Molecular and Biomolecular Spectroscopy

journal homepage: www.elsevier.com/locate/saa

Synthesis of trimethoprim metal complexes: Spectral, electrochemical, thermal, DNA-binding and surface morphology studies

Nihat Demirezen, Derya Tarınç, Duygu Polat, Mustafa Çeşme, Ayşegül Gölcü*, Mehmet Tümer

Department of Chemistry, Faculty of Science and Letters, University of Kahramanmaras Sutcu Imam, Campuse of Avsar, 46100 Kahramanmaras, Turkey

ARTICLE INFO

Article history:
Received 13 December 2011
Received in revised form 5 March 2012
Accepted 22 March 2012

Keywords:
Drug–metal complex
Trimethoprim
DNA binding
Voltammetry
PGE
SEM

ABSTRACT

Complexes of trimethoprim (TMP), with Cu(II), Zn(II), Pt(II), Ru(III) and Fe(III) have been synthesized. Then, these complexes have been characterized by spectroscopic techniques involving UV–vis, IR, mass and ^{1}H NMR. CHN elemental analysis, electrochemical and thermal behavior of complexes have also been investigated. The electrochemical properties of all complexes have been investigated by cyclic voltammetry (CV) using glassy carbon electrode. The biological activity of the complexes has been evaluated by examining their ability to bind to calf-thymus DNA (CT DNA) with UV spectroscopy and cyclic voltammetry. UV studies of the interaction of the complexes with DNA have shown that these compounds can bind to CT DNA. The binding constants of the complexes with CT DNA have also been calculated. The cyclic voltammograms of the complexes in the presence of CT DNA have shown that the complexes can bind to CT DNA by both the intercalative and the electrostatic binding mode. The antimicrobial activity of these complexes has been evaluated against three Gram-positive and four Gram-negative bacteria. Antifungal activity against two different fungi has been evaluated and compared with the reference drug TMP. Almost all types of complexes show excellent activity against all type of bacteria and fungi. The morphology of the CT DNA, TMP, metal ions and metal complexes has been investigated by scanning electron microscopy (SEM). To get the SEM images, the interaction of compounds with CT DNA has been studied by means of differential pulse voltammetry (DPV) at CT DNA modified pencil graphite electrode (PGE). The decrease in intensity of the guanine oxidation signals has been used as an indicator for the interaction mechanism.

1. Introduction

TMP, chemically 5-(3,4,5-trimethoxybenzyl)pyrimidine-2,4-diamine, the structure of which is shown in Fig. 1, belongs to the class of chemotherapeutic agents known as dihydrofolate reductase inhibitors. It is used in prophylaxis treatment and urinary tract infections [1].

The application of inorganic chemistry to medicine ("Elemental Medicine") is a rapidly developing field, and novel therapeutic and diagnostic metal complexes have an impact on medical practice. Advances in biocoordination chemistry are crucial for improving the design of compounds to reduce toxic side-effects and understand their mechanisms of action. Most of the major classes of pharmaceutical agents contain examples of metal compounds which are in current clinical use [2], and new areas of application are rapidly emerging. Some of these are discussed briefly below with special emphasis on the targeting of metal complexes and their bio-transformation. Targeting is important because the toxicity is often associated with metal compounds. If they can be delivered only to the tissues, cells and receptors where they are required, the toxicity may be reduced. The ease with which many metal complexes undergo ligand substitution and redox reactions is likely to mean that the active species are bio-transformation products of the administered complex. Identification of these active species will lead to the more effective use of metal compounds as drugs.

Compounds containing pyrimidine rings play a significant role in many biological systems [3]. The pyrimidine ring system, present in nucleic acids, several vitamins, coenzymes and antibiotics, provides potential binding sites for metal ions, and any information on their coordinating properties is important as a means of understanding the role of the metal ions in biological systems. Many compounds of therapeutic importance contain the pyrimidine ring system. So, substituted 2,4-diaminopyrimidines are widely employed as metabolic inhibitors of pathways leading to the synthesis of proteins and nucleic acids. Among these kinds of ligands, TMP is a well known biological agent, also employed as a potent metabolic inhibitor of bacterial dihydrofolic acid reductase. Trimethoprim has potential binding sites for metal ions. Several authors have studied the interaction of this ligand with biological

* Corresponding author. Tel.: +90 344 219 12 85; fax: +90 344 219 10 42.
E-mail addresses: agolcu@ksu.edu.tr, ag518@ksu.edu.tr (A. Gölcü).

1386-1425/$ – see front matter © 2012 Elsevier B.V. All rights reserved.
http://dx.doi.org/10.1016/j.saa.2012.03.055

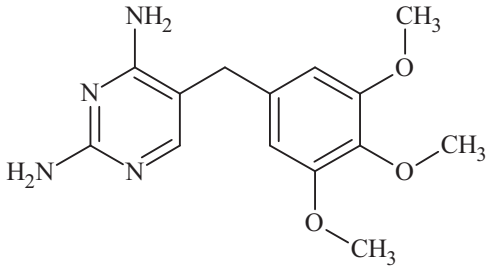

Fig. 1. The chemical structure of TMP.

metal ions and the coordination of TMP via a NH_2 nitrogen atom has been inferred on the basis of IR and visible measurements [4,5]. However, other authors have shown by X-ray diffraction methods that the coordination site of the TMP molecule is the N_1 of the pyrimidine ring [6–13]. On the other hand, more recently, other research groups [14–26] have prepared and characterized complexes of TMP with metal(II)/(III) and the spectral and analytical data show that the ligand acts as a monodentate or bidentate.

In this literature, the interactions of metal complexes of TMP with DNA have not been studied. Whereas, the study of the interactions of transition–metal complexes with DNA has been an active field of research. Interest in this field stems from attempts to gain some insight into the interaction model between DNA and the complexes, and obtain some information about drug design and tools of molecular biology [27]. Transition metal complexes can interact with DNA through a non-covalent way, such as electrostatic interaction, groove binding and intercalation. Binding to DNA through an intercalation mode with planar ligands intercalating into the adjacent base pairs of DNA [27] correlates to the planarity of the ligand, coordination geometry of the metal ion, and donor type of the ligand [28]. Considerable useful applications of these complexes need to be done to develop the complexes binding to DNA through an intercalation mode with their structures containing fully planar intercalating into the adjacent base pairs of DNA [27,28]. These give valuable information to explore the potential chemotherapeutical agents. Along this line, lots of copper(II) complexes, which possess biologically accessible redox potentials and demonstrate high nucleobase affinity, have been synthesized and their interactions with DNA extensively studied [29,30].

Electrochemical investigations of nucleic acid binding molecules–DNA interactions can provide a useful complement to the spectroscopic techniques and yield information about the mechanism at intercalation and the confirmation of anti bacterial–DNA adduct. The immobilization of DNA onto an electrode surface is crucial aspect in many ways of the developing DNA biosensors for monitoring drug (or complex) because it dictates the accessibility of the DNA to drug (or complex) in solution and hence can influence the affinity of drug binding. Binding of drug (or complex) to DNA and a general DNA damage has been described through the variation of the electrochemical signal of guanine or adenine [31,32]. Observing the electrochemical signal related to DNA–drug (or DNA-complex) interaction can provide evidence for the interaction mechanism and the nature of the complex formed, binding constant, size of binding site and the role of free radicals generated during interaction in drug (or complex) action. A good sensitivity of oxidation signals for DNA structure would make carbon electrodes extensively useful in DNA research especially pencil graphite electrode [33], carbon paste electrode [34] and glassy carbon electrode [35].

In this context, mononuclear metal(II/III) complexes have been synthesized and characterized. The complexes have been tested for their ability to bind to CT DNA. The binding properties of the complexes with CT DNA have been investigated with UV and CV titration.

2. Experimental

2.1. General

TMP was kindly provided by Glaxo Smith Kline Pharmaceutical Co. (Istanbul, Turkey). CT DNA was purchased from Sigma, NaCl, metal salts ($CuCl_2{\cdot}2H_2O$, $ZnCl_2$, $FeCl_3{\cdot}6H_2O$, K_2PtCl_4, and $RuCl_2{\cdot}3H_2O$), NaCl, 0.2 M Phosphate buffer at pH 2.0–12.0 and Tris–HCl were purchased from Merck. All the chemicals and solvents were reagent grade and were used as purchased. DNA stock solution was prepared by dilution of CT-DNA to buffer solution (containing 150 mM NaCl and 15 mM Tris–HCl at pH 7.0) followed by exhaustive stirring at 4 °C for three days [28], and kept at 4 °C for no longer than a week. The stock solution of CT-DNA gave a ratio of UV absorbance at 260 and 280 nm (A_{260}/A_{280}) of 1.89, indicating that the DNA was sufficiently free of protein contamination [27]. The DNA concentration was determined by the UV absorbance at 260 nm after 1:20 dilution using $\varepsilon = 6600\ M^{-1}\ cm^{-1}$ [29]. Elemental analyses (C, H and N) were performed using a LECO CHNS 932 elemental analyser. Infrared spectra of the ligands and their metal complexes were obtained using KBr discs (4000–400 cm^{-1}) with a Perkin Elmer spectrum 400 FT-IR spectrophotometer. Far spectra of the complexes were recorded using a Perkin Elmer spectrum 400 FT-IR/FT-FAR instrument. The electronic spectra were obtained in the 200–900 nm range by a Perkin Elmer Lambda 45 spectrophotometer. Magnetic measurements were carried out by the Gouy method using $Hg[Co(SCN)_4]$ as a calibrant. Mass spectra of the ligands were recorded on a LC/MS APCI AGILENT 1100 MSD spectrophotometer. ^1H NMR spectra were recorded on a Bruker 400 MHz instrument. TMS was used as internal standard and DMSO as solvent. The metal content of the complex was determined by an Ati Unicam 929 Model AA Spectrometer in solutions prepared by decomposing the compounds in aqua regia and then subsequently digesting in concentrated HCl. The thermal analysis studies of the complexes were performed on a Perkin Elmer STA 6000 simultaneous Thermal Analyzer under nitrogen atmosphere at a heating rate of 10 °C/min. Scanning electron micrography associated with SEM Neo Scope JSM-5000 was used for morphological evaluation.

2.2. Electrochemical measurements

All voltammetric measurements at the glassy carbon working electrode was performed using a BAS 100 W (Bioanalytical System, USA) electrochemical analyzer. Glassy carbon working electrode (BAS; Φ: 3 mm diameter), an Ag/AgCl reference electrode (BAS; 3 M KCl) and platinum wire counter electrode and a standard one-compartment three electrode cell of 10 mL capacity were used in all experiments. Glassy carbon working electrode was polished manually with aqueous slurry of alumina powder (Φ: 0.01 μm) on a damp smooth polishing cloth (BAS velvet polishing pad), before each measurement. All measurements were realized at room temperature. Mettler Toledo MP 220 pH meters was used for the pH measurements using a combined electrode (glass electrode reference electrode) with an accuracy of ±0.05 pH.

2.3. Synthesis of a copper(II), zinc(II), platinum(II), iron(III) and ruthenium(III) complex

All metal complexes have been obtained according to a general procedure: a solution of a metal salt (1 mmol) dissolved in 5 mL of MeOH have been added to a solution of TMP ligand (1 mmol) in 5 mL of distilled water and finally 15 mL of MeOH have been added to mixture and the mixture have been heated under reflux

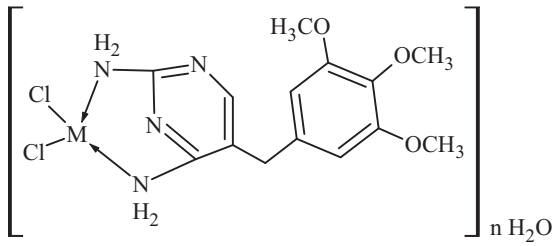

Fig. 2. Proposed structure of Cu(II), Zn(II) and Pt(II) complexes ($n = 0$ for Cu(II), $n = 3$ for Pt(II) and $n = 1$ for Zn(II) complexes).

for one day. At the end of the reaction, determined by TLC, the precipitate have been filtered off, washed with distilled water, EtOH and dried under vacuum. The proposed formulas of M(II)–TMP and M(III)–TMP complexes have been given in Figs. 2 and 3, respectively.

2.4. Preparation of the microorganism cultures

The growth inhibitory activity of the chemical matter has been tested against ten bacteria (*Eschericha coli*, *Enterobacter cloaca*, *Bacillus megaterium*, *Bacillus cereus*, *Pseudomonas* sp., *Brusella melitensis*, *Saccharomyces cerevicia* and *Staphylococcus aureus*) and fungi (*Candida albicans* and *Saccharomyces cerevicia*). These microorganisms have been provided from Microbiology Laboratory Culture Collection, Department of Biology, Kahramanmaras Sutcu Imam University, Kahramanmaras, Turkey. Antimicrobial activities of the chemical matter have been determined using the agar-disc diffusion method as described below. The bacteria have been first incubated at 37 ± 0.1 °C for 24 h in nutrient broth (Difco), and the yeasts have been incubated in sabouraud dextrose broth (Difco) at 25 ± 0.1 °C for 24 h. The cultures of the bacteria and yeast have been injected into the petri dishes (9 cm) in the amount of 0.1 mL. And then, mueller hinton agar) and sabouraud dextrose agar (sterilized in a flask and cooled to 45–50 °C) have been homogenously distributed onto the sterilized petri dishes in the amount of 15 mL. Subsequently, the sterilized blank paper discs of 6 mm diameter have been saturated with 1200 μg of chemical matters per disc. The discs have been placed onto the agar plates, which had previously been inoculated with the above organisms. In addition, blank paper discs treated with TMP has been used as positive controls. Afterwards the plates combined with the discs have been left at 4 °C for 2 h, the plates injected with yeast have been incubated at 25 ± 0.1 °C for 24 h, and ones injected with bacteria have been incubated at 37 ± 0.1 °C for 24 h. After 24 h, inhibition zones appearing around the discs have been measured and recorded in mm. The initial number of microorganisms in the suspension has been determined for the total yeasts and bacterial count during 24 h at 37 °C for bacteria and 48 h 25 °C for yeasts [36].

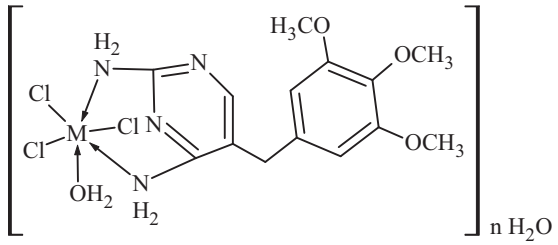

Fig. 3. Proposed structure of Ru(III) and Fe(III) complexes ($n = 0$ for Fe(III) and $n = 1$ for Ru(III) complexes).

2.5. DNA-binding studies

The interaction of the complexes with CT DNA has been studied with UV spectroscopy and CV in order to investigate the possible binding modes to CT DNA and to calculate the binding constants to CT DNA (K_b). In UV titration experiments, the spectra of CT DNA in the presence of complex has been recorded for a constant CT-DNA concentration in diverse [complex]/[CT DNA] mixing ratios (r). The intrinsic binding constant, K_b, of the complex with CT DNA has been determined through the UV spectra of the complex recorded for a constant complex DNA concentration (4.2×10^{-8} M) in the absence and presence of CT DNA for diverse r values [27]. The interaction of the complex with CT DNA has also been investigated by monitoring the changes observed in the cyclic voltammogram of a 3×10^{-4} M buffer solution of the complex upon addition of CT DNA at diverse r values. The buffer has also been used as the supporting electrolyte and the cyclic voltammograms have been recorded at $m = 100$ mV/s.

2.6. Morphology studies

Pencil graphite electrode (PGE) used for morphology studies. So, DPV has been performed with an Autolab-PGSTAT 30 electrochemical analysis system with a General Purpose Electrochemical Software (mlS) 4.9 software package (Eco Chemie, Utrecht, The Netherlands). The three electrode system consisted of the PGE, as the working electrode, a reference electrode (Ag/AgCl) and a platinum wire as the auxiliary electrode. The renewable PGE process has been described in literature 37 [37]. A Noki® pencil has been used as a holder for Pentel® graphite leads. The pencil has been hold vertically with 15 mm of the lead extruded outside (12 mm of which was immersed in the solution) [38]. Each measurement has been performed using a new graphite lead. PGE has been activated at +1.40 V for 1 min in 0.50 M Tris–HCl buffer solution for electrode surface pretreatment. The CT DNA has been immobilized onto the pre-treatment PGE surface by applying a potential at +0.50 V during 240 s using 400 rpm stirring rate in 0.50 M Tris–HCl buffer containing 4.00 μg/mL CT DNA. Then, the electrode has been cleaned with blank acetate buffer solution for 5 s for the removal of the unbound CT DNA at the electrode surface. The CT DNA has been immobilized and PGE has been immersed into Tris-buffer solution (30% ethanol) containing same concentrations of compound (TMP or M(II)/(III) complexes) during 180 s with 400 rpm stirring at open circuit system. Then, the electrode has been rinsed with blank Tris–HCl buffer solution for 5 s and SEM images have been recorded. All SEM images have been taken on carbon strip.

3. Results and discussion

In this study, metal(II/III) complexes of TMP have been prepared and characterized by the analytical and spectroscopic methods. The isolated complexes are stable in air, insoluble in water and common organic solvents, but completely soluble in DMSO. The elemental analysis, color, and melting point together with the formula weight obtained from the mass spectra for the complexes are given in Table 1 and agree very well with molecular formula proposed. The analytical data show the composition of the metal complexes to be $[Cu(Cl)_2(TMP)]$, $[Zn(Cl)_2(TMP)]\cdot(H_2O)$, $[Pt(Cl)_2(TMP)]\cdot 3(H_2O)$, $[Fe(Cl)_3(TMP)(H_2O)]$ and $[Ru(Cl)_3(TMP)(H_2O)]\cdot(H_2O)$. The ratios of the metal present in all complexes have been determined by atomic absorption spectroscopy. The complexes have been decomposed in HNO_3/H_2O_2 (1/1) and then dissolved in 1.5 N HNO_3. The amounts of metals have been determined (Table 1). They support the structures given in Figs. 2 and 3. The molar conductivity measurements have been done all compounds in DMSO ($\sim 1.10^{-3}$ M solutions). The conductivity data of the complexes are very low and they can be

Table 1
Analytical and physical properties of trimethoprim complexes.

Compound	Formula weight (g/mol)	Color	Yield (%)	Freezing point (°C)	Elemental analysis; calculated (found)			
					C	H	N	M
$[Cu(Cl)_2(TMP)]$	424.76	Green	72	194	39.59 (41.14)	4.27 (4.86)	13.19 (13.34)	14.95 (14.13)
$[Ru(Cl)_3(TMP)(H_2O)]\cdot(H_2O)$	551.79	Black	80	263	30.47 (30.21)	4.38 (4.11)	10.15 (9.50)	18.43 (19.03)
$[Fe(Cl)_3(TMP)(H_2O)]$	470.53	Brown	73	240	35.74 (35.09)	4.28 (4.36)	11.91 (11.29)	11.86 (11.69)
$[Zn(Cl)_2(TMP)]\cdot(H_2O)$	444.64	White	66	174	37.82 (38.09)	4.53 (4.46)	12.60 (12.34)	14.70 (14.54)
$[Pt(Cl)_2(TMP)]\cdot 3(H_2O)$	610.35	Black	64	271	27.55 (27.50)	3.96 (3.12)	9.18 (8.62)	31.96 (30.98)

regarded as non-electrolytes. Chloride ions in the all complexes have been determined by titration with $AgNO_3$.

Diverse crystallization techniques have been employed in order to obtain a crystal suitable for the structure determination with X-ray crystallography. Nevertheless, the complexes have been collected as microcrystalline products.

The formation of the complexes also confirmed by UV–vis spectra (Table 2). In the UV–vis measurements, acetonitrile/water (1/1, v/v) have been used as a solvent. All complexes except Pt(II) and Zn(II) complexes, shows d–d transitions between 409 and 603 nm [39]. The spectra of the complexes show bands between 378 and 396 nm assigned to M→L and L→M (L: ligand, M: metal) charge transfer transitions. There are n→(* and (→(* transitions between 325–374 and 233–296 nm, respectively.

The magnetic moments (as BM) of the complexes have been measured at room temperature. The Zn(II) and Pt(II) complexes have the diamagnetic character while the Zn(II) complex has tetrahedral geometry, the Pt(II) complex is square-planar around the metal ion. The structures of the mononuclear Cu(II) complex are supported by the magnetic moment data. The measured magnetic moment value of the Cu(II) complex of the TMP is 1.80 BM, which is very close to that of the spin only value (1.73 BM) expected for a complex having one copper(II) ion with a single unpaired electron located in an essentially $d_{x^2-y^2}$ orbital. This value suggests that the copper atom is in a square planar environment in its chelates [40]. The observed magnetic moment of Fe(III) complex is 5.20 BM. Thus, the complex formed has the octahedral geometry. Magnetic susceptibility measurement of the Ru(III) complex at 298 K showed a value of e.m.u.g^{-1} with an effective magnetic moment μ_{eff} of 1.95 BM. The μ_{eff} value is slightly smaller than the spin-only moment of an unpaired electron. Thus, it can be concluded that a change in the formal oxidation state of the ruthenium atom from 0 to +1 has been achieved via oxidative addition of the —NH_2 groups to ruthenium. This situation explores that a proton displacement to give a low-spin d^7 electronic configuration, Fig. 3. An effective magnetic moment of 1.95 BM for this complex and the assignment of the spectra are in conformity with the octahedral geometry.

In order to clarify the mode of bonding and the effect of the metal ion on the ligand, the FT-IR spectra of the TMP and metal complexes have been compared and assigned on the basis of careful comparison. The FT-IR spectra of TMP and its metal complexes are listed in Table 3 and Fig. 4a and b. TMP possesses seven potential donor sites; two pyrimidinyl N atoms, two NH_2 groups on the pyrimidine rings and three methoxy groups. So, the ν_{as}(N—H) and ν_s(N—H) modes of the pyrimidine-NH_2 groups in the free TMP are assigned to the strong and sharp bands at 3469 and 3317 cm^{-1}, respectively, which are affected by the presence of hydrogen bonds [40]. In all the complexes the bands ν(N—H), due to asymmetric and symmetric vibrations, are present in the region 3482–3405 cm^{-1}; these bands shifted significantly with respect to those of the ligand. This confirms that the metal ion is coordinated to the trimethoprim through the two N atoms that belong to NH_2 groups. ν(C=N) of conjugated cyclic system of the ligand is lowered in complex with respect to ligand. This is an indication of bonding of metal

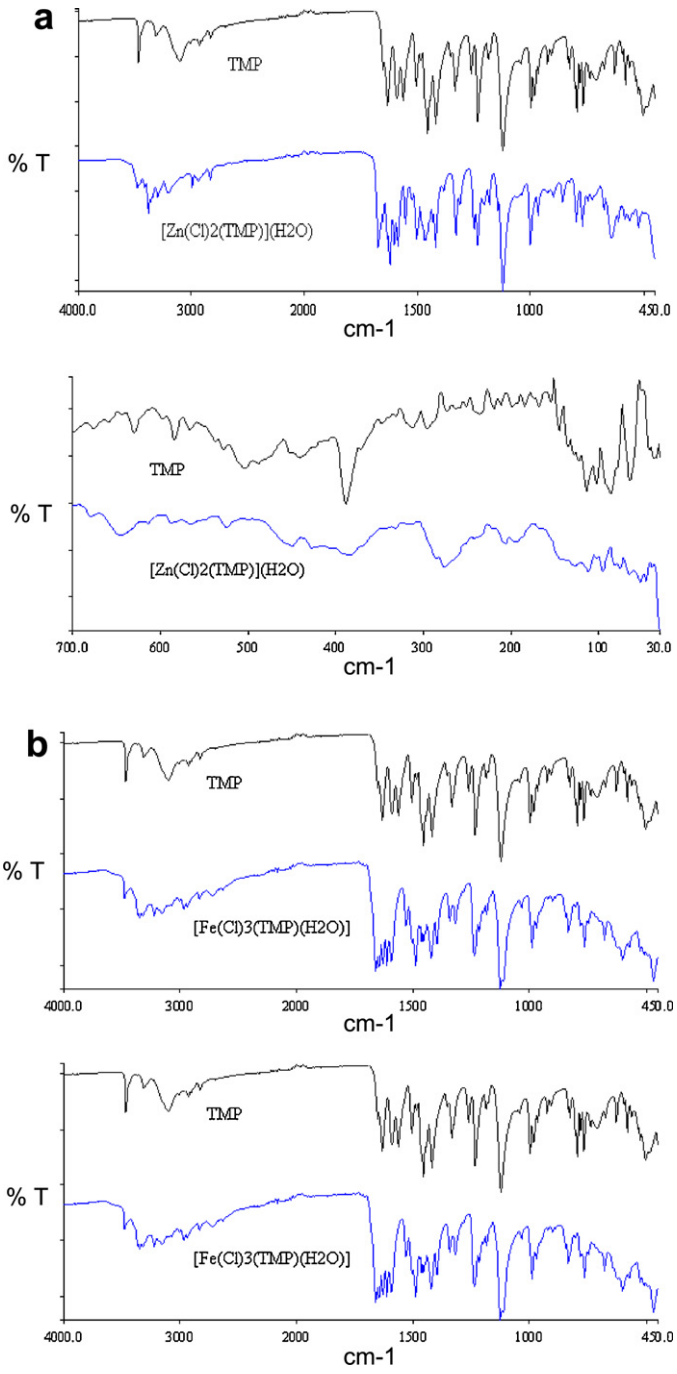

Fig. 4. The infrared spectra of the $[Zn(Cl)_2(TMP)]\cdot(H_2O)$ (a) and $[Fe(Cl)_3(TMP)(H_2O)]$ (b) complexes.

Table 2
Spectroscopic data of TMP metal complexes.

Compound	π–π^* (nm)	n–π^* (nm)	Charge transfer (nm) (M→L or L→M)	d–d* (nm)
$[Cu(Cl)_2(TMP)]$	274	334	381	603
$[Ru(Cl)_3(TMP)(H_2O)]\cdot(H_2O)$	252	341	396	409
$[Fe(Cl)_3(TMP)(H_2O)]$	264	374	379	559
$[Zn(Cl)_2(TMP)]\cdot(H_2O)$	233	338	378	–
$[Pt(Cl)_2(TMP)]\cdot 3(H_2O)$	296	325	379	–

Table 3
FAR-and MID-IR results of TMP and its metal complexes.

Compound	ν_{as}(N—H)	ν_s(N—H)	ν(C=N)	ν(M—N)	ν(M—O)	ν(M—Cl)
TMP	3469	3317	1652	–	–	–
$[Cu(Cl)_2(TMP)]$	3451	3405	1640	605	–	264
$[Ru(Cl)_3(TMP)(H_2O)]\cdot(H_2O)$	3469	3400	1641	473	366	274
$[Fe(Cl)_3(TMP)(H_2O)]$	3478	3353	1629	605	472	263
$[Zn(Cl)_2(TMP)]\cdot(H_2O)$	3482	3386	1602	645	–	274
$[Pt(Cl)_2(TMP)]\cdot 3(H_2O)$	3547	3323	1632	471	–	261

ion through two–NH_2 nitrogen of conjugated cyclic system. In order to investigate the substituent effect upon both the δ- and π-contribution to the total metal–nitrogen and metal–chloride bond strength, the FT-Far method have been used. Furthermore, the effect of the substituents on the metal–halogen bond of the TMP metal complexes has also been examined. The infrared spectra in the region 700–30 cm^{-1} have been measured for the complexes, and the maximum absorption frequencies are listed in Table 3. The spectra of the $[Zn(Cl)_2(TMP)]\cdot(H_2O)$ and $[Fe(Cl)_3(TMP)(H_2O)]$ complexes are given in Fig. 4a and b, respectively. The far spectra of all complexes of the TMP have similar features, they are characterized by two or three strong metal–chlorine stretching bands and two medium metal–nitrogen (ligand) stretching bands in this region. Therefore, it can be reasonably assumed that the substituents (—NH_2 groups) on the meta-position of the formyl ring change the stereo-configuration of the metal complexes. On the whole, analogous to the case of the copper(II) complexes, the metal-chlorine stretching (metal: Zn(II), Pt(II) Fe(III) and Ru(III)) frequencies due to the effects of both electron-releasing and electron-attracting substituents. This phenomenon is apparently due to the delocalized nature of the coordination bonds in the complexes. In the complexes, the ν(M—Cl) stretching frequency has been seen in the 274–261 cm^{-1} range. The ν(M—N) stretching frequencies have been shown in the 471–645 cm^{-1} range. The ν(M—O) stretching frequencies in $[Fe(Cl)_3(TMP)(H_2O)]$ and $[Ru(Cl)_3(TMP)(H_2O)]\cdot(H_2O)$ complexes have been seen in 472 cm^{-1} and 366 cm^{-1}, respectively.

The formulation of the complexes are deduced from analytical data, ^1H NMR and further supported by mass spectroscopy. The relatively low intensities of the molecular ion peaks, $[M]^+$, are indicative of the ease of fragmentation of the complexes, and this may reflect the number of heteroatoms present in each structure. The spectra of the ruthenium complex shows peak at m/e 533. This peak can attribute to the molecular ion peaks $[M]^+$. All the compounds decompose in a similar way. In the mass spectra of the ruthenium complex, the highest intensity peaks are at m/e 415 (100%) may be assigned to the $[M—CH_3O_2Cl_2]^+$ ions which is formed by the loss of other parts of the molecular ions. Typical mass spectrum of $[RuCl_3(TMP)(H_2O)]\cdot(H_2O)$ is given in Fig. 5.

The ^1H NMR spectra of the TMP and its complexes have been recorded using DMSO and obtained results are given in Table 4. In the spectrum of the TMP, the–CH_2 protons are seen at 3.40 ppm as singlet. The singlets in the 3.72 and 3.52 ppm can be attributed to the methoxy protons. The slightly broad bands at the 5.71 and 6.10 ppm can be attributed to the —NH_2 protons. The aromatic protons are shown at 6.55 and 7.51 ppm as singlets. In the spectra of the complexes, the —NH_2 protons have been shifted to the lower regions and this situation confirms that the nitrogen atom of the amines group coordinates to the metal ions. Typical NMR spectra of TMP and its zinc complex are given in Fig. 6a and b, respectively.

Thermal studies of all the complexes were performed under nitrogen atmosphere in the temperature range of 20–1000 °C. The thermal curves of the $[Pt(Cl)_2(TMP)]\cdot 3(H_2O)$ and $[Fe(Cl)_3(TMP)(H_2O)]$ complexes are given in Fig. 7a and b. All complexes (except copper(II) complex) have the adsorbed and/or hydrated water molecules. As seen from Fig. 7 and the figures of the other complexes, the hydrated water molecules have been eliminated at the first step in the 30–100 °C temperature range. The intermediates are stable within the interval of 135–240 °C. The loss of the hydrated water molecules has been seen as endothermic peaks in the DTA curves. While the iron(III) and ruthenium(III) complexes contain the coordinated water molecules and chloride ions, zinc(II) and platinum(II) complexes contain only coordinated chloride ions. Coordinated water molecules in the Fe(III) and Ru(III) complexes eliminate within the temperature range of 100–200 °C. The coordinated chloride ions in the complexes, loss from the molecule in the 240–400 °C temperature range [41]. This process is connected with the elimination of one and or two coordinated chloride ions and the formation of [M(L)] specie which is thermally stable up to the higher temperatures. Main mass losses are at the higher temperatures. Then, the mass of the samples decreased slightly up to 1000 °C. From the calculations, it follows that the final decomposition product can be MO/M_2O_3 (MO is for the Cu(II), Zn(II) and Pt(II) complexes; M_2O_3 is for the Ru(III) and Fe(III) complexes).

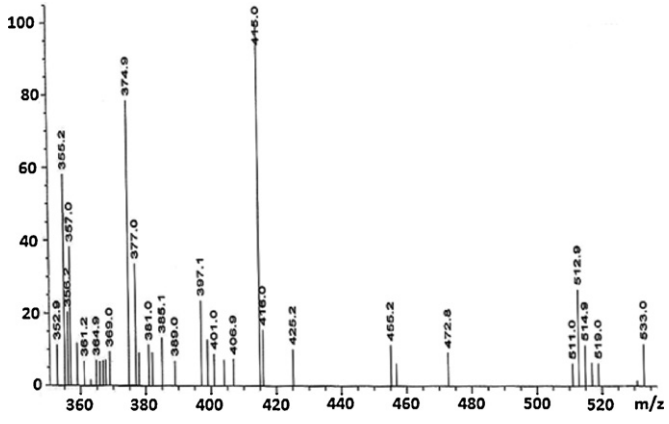

Fig. 5. Mass spectrum of the $[RuCl_3(TMP)(H_2O)]\cdot(H_2O)$.

Table 4
The NMR results of TMP and its Zn(II) and Pt(II) complexes.

Compound	—CH_2	—OCH_3	—NH_2	Ar—H
TMP	3.40 (s, 2H)	3.52, 3.72 (s, 6H)	5.71, 6.10 (s, 4H)	6.55, 7.51 (m, 2H)
$[Zn(Cl)_2(TMP)]\cdot(H_2O)]$	3.42 (s, 2H)	3.72, 3.90 (s, 6H)	6.43, 6.74 (s, 4H)	6.99, 7.44 (m, 2H)
$[Pt(Cl)_2(TMP)]\cdot 3(H_2O)]$	3.43 (s, 2H)	3.62, 3.74	6.43, 6.70	6.96, 7.46 (m, 2H)

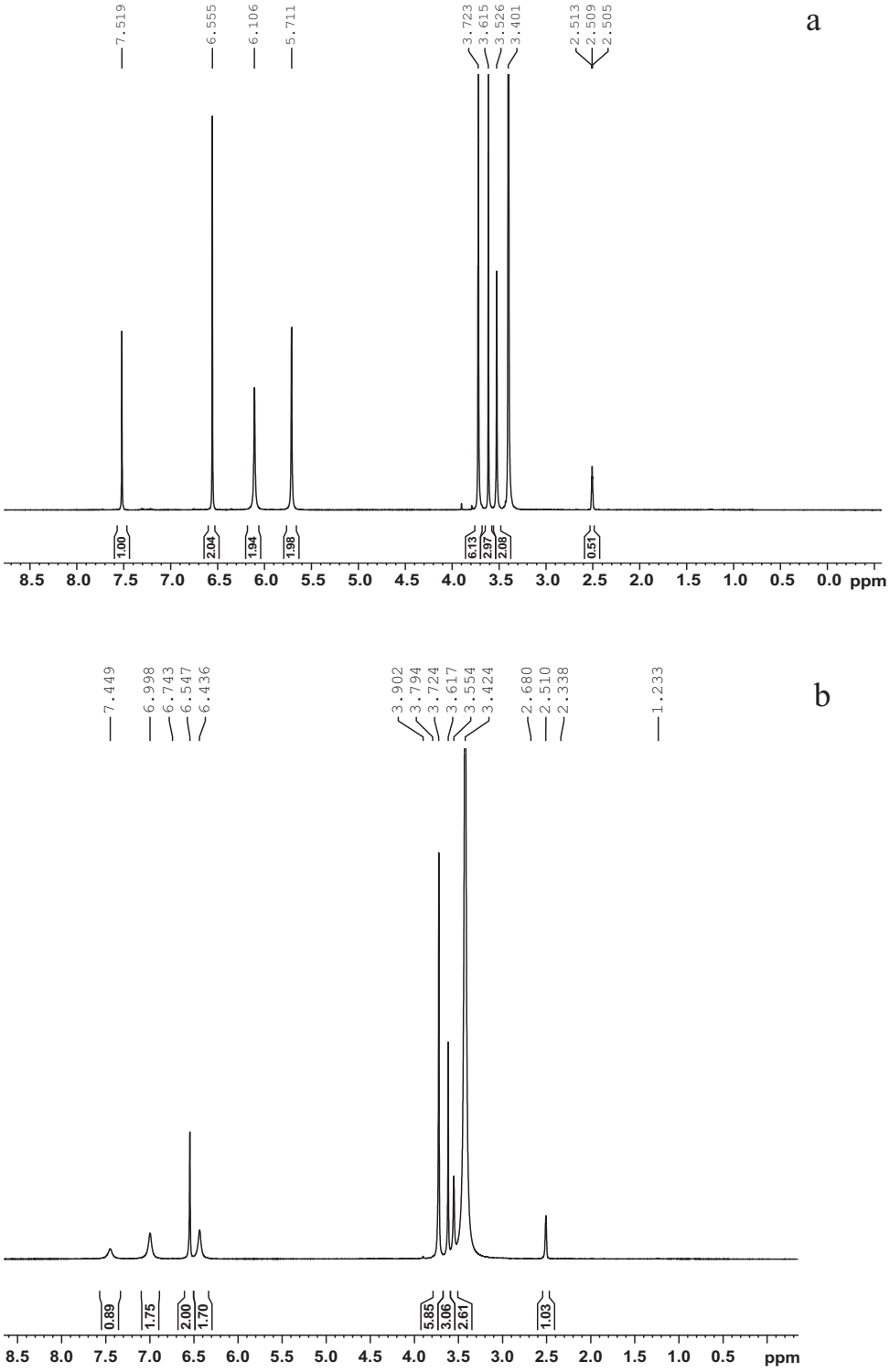

Fig. 6. NMR spectra of TMP (a) and $[Zn(Cl)_2(TMP)]\cdot(H_2O)$ complex (b).

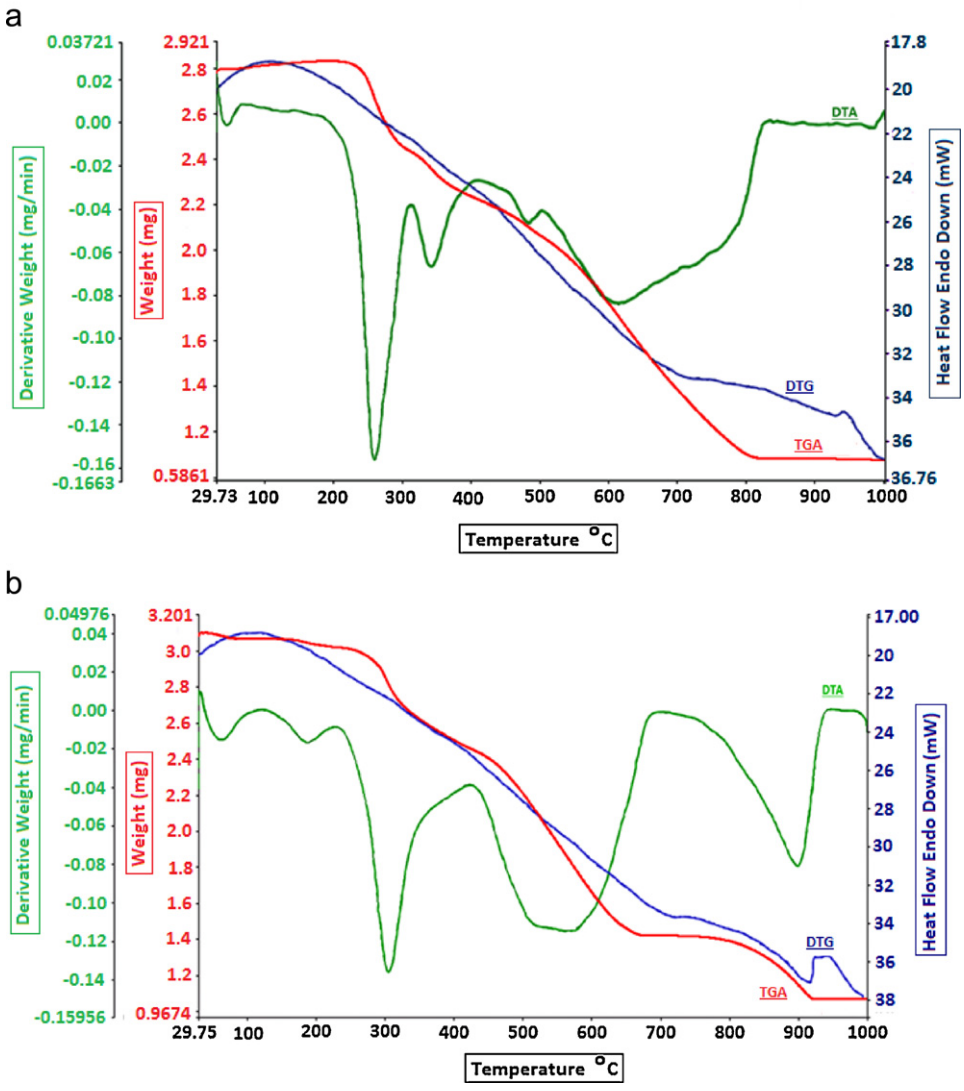

Fig. 7. The thermal curves of the $[Fe(Cl)_3(TMP)(H_2O)]$ (a) and $[Pt(Cl)2(TMP)]\cdot 3(H_2O)$ (b) complexes.

In this research, TMP and its be $[Cu(Cl)_2(TMP)]$, $[Zn(Cl)_2(TMP)]\cdot(H_2O)$, $[Pt(Cl)_2(TMP)]\cdot 3(H_2O)$, $[Fe(Cl)_3(TMP)(H_2O)]$ and $[Ru(Cl)_3(TMP)(H_2O)]\cdot(H_2O)$ complexes have been subjected to a cyclic voltammetric study with the aim of the detailed characterizing their electrochemical behavior, on the glassy carbon electrode. Therefore, the electrochemical behaviors of compounds have been studied over a wide pH range (2–12.0) with a glassy carbon disc electrode in phosphate buffered aqueous media.

In earlier studies, Kotoucek et al. [42] evaluated the mechanism of the polarographic reduction of TMP. In their study, in concentrated sulfuric acid ($c > 0.1\ mol\ dm^{-3}$) the protonized TMP has been reduced in a two-electron process. In this study, cyclic voltammetric technique has been used. In CV studies, the scanning has been started at +1.5 V in the positive direction, the anodic oxidation of TMP does not occur until about 0.0 V for GCE. After 0.0 V, TMP yields one well-defined peak and one ill-defined peak has been observed on the cathodic branch for GCE at −0.22 V (4.2×10^{-6} A for 3×10^{-4} M TMP solution) and −0.60 V (8.8×10^{-7} A for 3×10^{-4} M TMP solution), respectively. When examined of CV behavior of all metal complexes in same medium, peak at −0.3 V is shifted more positive potential values and its current increased (+0.14 V, 5.7×10^{-6} A for $[Cu(Cl)_2(TMP)]$, (+0.16 V, 5.9×10^{-6} A for $[Zn(Cl)_2(TMP)]\cdot(H_2O)$, +0.20 V, 6×10^{-6} A for $[Pt(Cl)_2(TMP)]\cdot 3(H_2O)$, +0.10 V, 4×10^{-6} A for $[Fe(Cl)_3(TMP)(H_2O)]$ and (+0.13 V, 5.3×10^{-6} $[Ru(Cl)_3(TMP)(H_2O)]\cdot(H_2O)$ and all complexes are 3×10^{-4} M). Fig. 8 shows comparative CV of TMP in the presence of copper(II) ions at cathodic directions for: (a) blank, (b) TMP alone, (c) $[Cu(Cl)_2(TMP)]$. In the figure (Fig. 8c) of the $[Cu(Cl)_2(TMP)]$ complex as different from the CV curve (Fig. 8b) of the TMP drug. The cathodic peak at +0.14 V shows the reduction of the Cu(II) ion. This process is: $Cu(II) + e^- \rightarrow Cu(I)$. In addition, the anodic peak at +0.08 V is the oxidation peak of the $[Cu(Cl)_2(TMP)]$ complex. This is $Cu(I) \rightarrow Cu(II) + e^-$. The oxidation and reduction process are irreversible.

The pH of the supporting electrolyte has a significant effect on the electro-reduction of the complexes at the GCE. Plots of pH vs. E_p and I_p have been investigated using CV techniques. The peak potential (E_p) at the redox process moved to less positive potential values by raising the pH (Fig. 9).

The plot of the peak potential vs. pH shows one straight line between pH 2.0 and 12.0, which can be expressed by the following equations in phosphate buffer:

$$E_p\,(mV) = -119.5\text{–}2.5\,pH;$$

$$r = 0.94498528 \text{ for } [Cu(Cl)_2(TMP)] \quad (pH = 2\text{–}4)$$

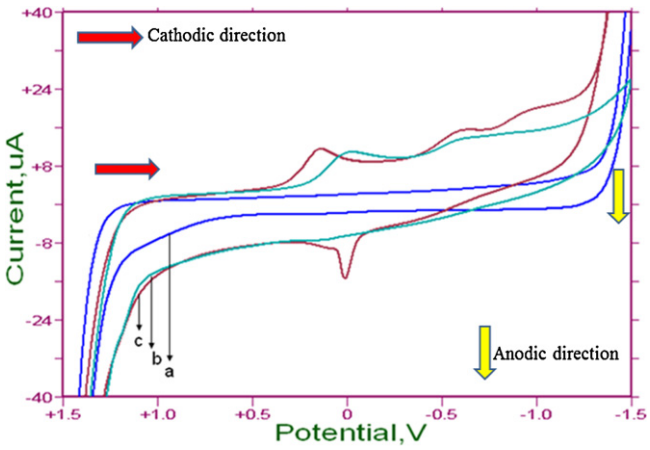

Fig. 8. Cyclic voltammogram of TMP in the presence of copper(II) ions at cathodic directions for: (a) Supporting electrolyte, (b) 3×10^{-4} M TMP, (c) 3×10^{-4} M $[Cu(Cl)_2(TMP)]$. Initial potential: 1500 mV, high potential: 1500 mV, low potential: −1500 mV, scan rate: 100 mV/s, sensitivity: 10 μA/V, number of the segments: 2.

$$E_p\,(\mathrm{mV}) = 1318.1 - 21.84\,\mathrm{pH};$$
$$r = 0.9549 \text{ for } [Zn(Cl)_2(TMP)]\cdot(H_2O) \quad (\mathrm{pH} = 2\text{–}12)$$

$$E_p\,(\mathrm{mV}) = 1409 - 29.38\,\mathrm{pH};$$
$$r = 0.9720 \text{ for } [Pt(Cl)_2(TMP)]\cdot 3(H_2O) \quad (\mathrm{pH} = 2\text{–}12)$$

$$E_p\,(\mathrm{mV}) = 2807.3 - 152\,\mathrm{pH};$$
$$r = 0.9858 \text{ for } [Ru(Cl)_3(TMP)(H_2O)]\cdot(H_2O) \quad (\mathrm{pH} = 9\text{–}12)$$

$$E_p\,(\mathrm{mV}) = 1330.2 - 23.15\,\mathrm{pH};$$
$$r = 0.9304 \text{ for } [Fe(Cl)_3(TMP)(H_2O)] \quad (\mathrm{pH} = 2\text{–}12)$$

The effects of pH on peak current of all complexes in the range of pH 2.0–12.0 have also been evaluated. The best and sharpest peak and reproducible results (except $[Ru(Cl)_3(TMP)(H_2O)]\cdot(H_2O)$ complex) have been obtained in pH 2.0 phosphate buffer. pH 9 is best media for $[Ru(Cl)_3(TMP)(H_2O)]\cdot(H_2O)$ complex. Therefore these mediums have been chosen in this study as the supporting electrolyte for the electroanalytical investigations. Scan rate studies have been carried out to investigate whether the process at the GCE is under diffusion or adsorption control. The effect of the potential scan rate between 5 mV/s and −500 mV/s on the peak current and potential of all complexes have been evaluated in pH 2 or 9 phosphate buffer. The typical current–potential curve of scan rate studies of $[Cu(Cl)_2(TMP)]$ complex has been given in Fig. 10. When the scan rate has been varied from 5 to 500 mV/s in 1×10^{-4} M complex solutions, a linear dependence of the peak current I_p (μA) upon the square root of the scan rate $v^{1/2}$ (mV/s) was found by GCE, demonstrating a diffusional behavior.

The effect of scan rate on peak current has also been examined under the above conditions with a plot of logarithm of peak current vs. logarithm of scan rate giving a straight line within the same scan rate range. These linear relationships have been obtained as follow (n = 10 in all studies):

$$\log I_p\,(\mu\mathrm{A}) = 0.3650 \log v\,(\mathrm{mV/s}) - 0.315$$
$$r\text{: } 0.9900 \text{ for } [Cu(Cl)_2(TMP)]$$

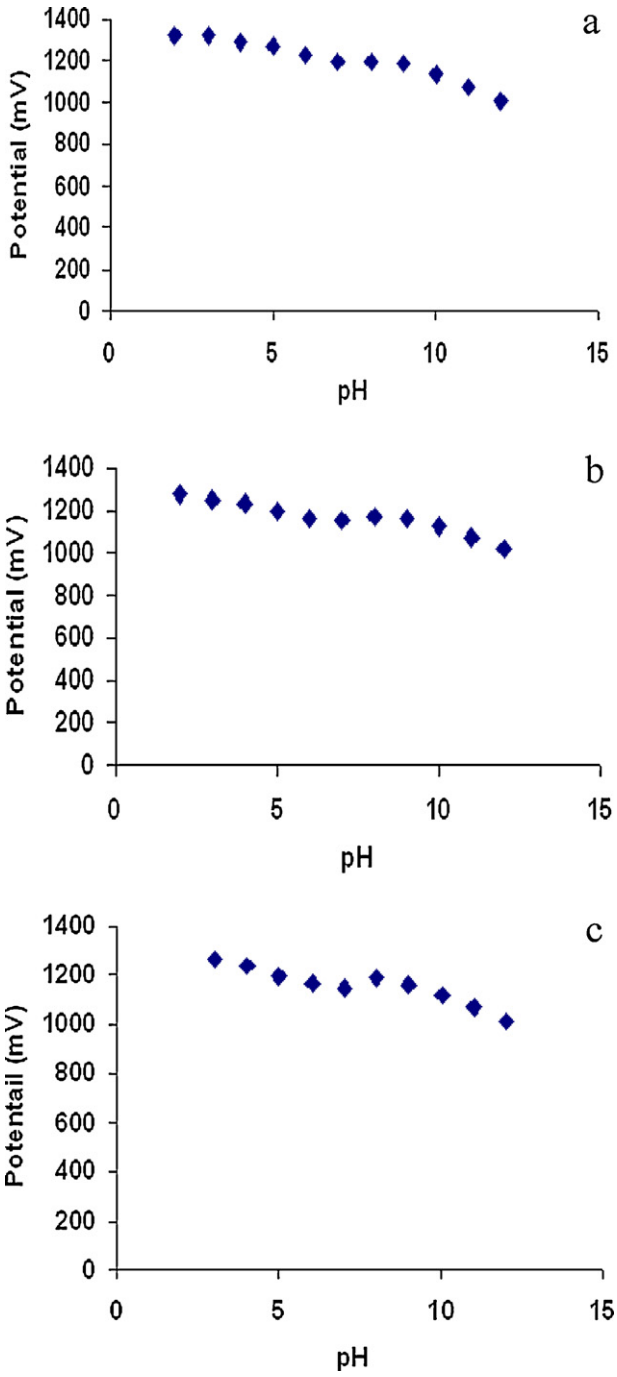

Fig. 9. Effects of pH on [Pt(Cl)2(TMP)]·3(H_2O) (a), $[Zn(Cl)_2(TMP)]\cdot(H_2O)$ (b), and $[Fe(Cl)_3(TMP)(H_2O)]$ (c) anodic peak potential, complex concentration 1×10^{-4} M and 0.2 M phosphate buffers.

$$\log I_p\,(\mu\mathrm{A}) = 0.6477 \log v\,(\mathrm{mV/s}) - 0.6491$$
$$r\text{: } 0.9969 \text{ for } [Zn(Cl)_2(TMP)]\cdot(H_2O)$$

$$\log I_p\,(\mu\mathrm{A}) = 0.4821 \log v\,(\mathrm{mV/s}) - 0.0032$$
$$r\text{: } 0.9960 \text{ for } [Pt(Cl)_2(TMP)]\cdot 3(H_2O)$$

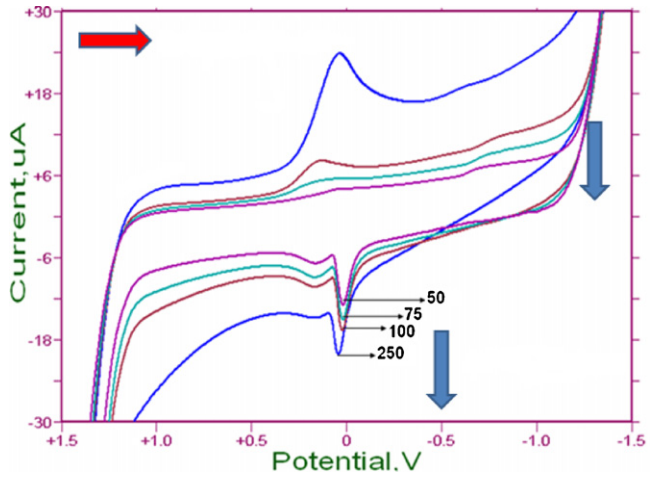

Fig. 10. The scan rate (5–500 mV/s) effect on peak current of $[Cu(Cl)_2(TMP)]$ complex.

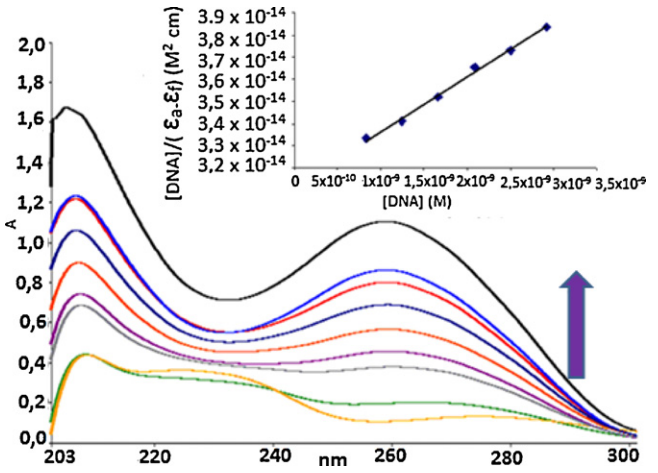

Fig. 11. UV spectra of $[Cu(Cl)_2(TMP)]$ in buffer solution in the presence of CT DNA at increasing amounts. $[Cu(Cl)_2(TMP)] = 1 \times 10^{-5}$ M. The arrow shows the intensity changes upon increasing concentration of CT DNA.

$$\log I_p\,(\mu A) = 0.4774 \log \nu\,(mV/s) - 0.2572$$
$$r\text{: } 0.9968 \text{ for } [Fe(Cl)_3(TMP)(H_2O)]$$

$$\log I_p\,(\mu A) = 0.2750 \log \nu\,(mV/s) + 0.4593$$
$$r\text{: } 0.9842 \text{ for } [Ru(Cl)_3(TMP)(H_2O)]\cdot(H_2O)$$

The slopes (between 0.27 and 0.64) of the relationship are close to the theoretically expected (0.5) for an ideal reaction of solution species, so in this case the process has a diffusive component [43–45].

The mutual effect of the complexes with CT DNA has been studied with UV spectroscopy and CV in order to investigate the possible binding modes to CT DNA and to calculate the binding constants to CT DNA (K_b). In UV titration experiments, the spectra of CT DNA in the presence of each complexes (or TMP) have been recorded for a constant CT DNA concentration in diverse [complex (or TMP)]/[CT DNA] mixing ratios (r). The intrinsic binding constants, K_b, of the complexes (or TMP) with CT DNA have been determined through the UV spectra of the complexes recorded for a constant complex (or TMP) DNA concentration (4×10^{-5} M) in the absence and presence of CT DNA for diverse r values. The interaction of the complexes (or TMP) with CT DNA has been also investigated by monitoring the changes observed in the cyclic voltammogram of a 1×10^{-5} M (1/9 methanol/buffer solution containing) of the complexes upon addition of CT DNA at diverse r values. The transition metal complexes are known to bind to DNA via both covalent and/or noncovalent interactions [27,29,31,46]. In covalent binding the labile ligand of the complexes is replaced by a nitrogen base of DNA such as guanine N_7. Moreover, the noncovalent DNA interactions include intercalative, electrostatic and groove (surface) binding of metal complexes along outside of DNA helix, along major or minor groove. It has been reported that DNA can provide three distinctive binding sites for all metal complexes; namely, groove binding, electrostatic binding to phosphate group and intercalation [47]. This behavior is of great importance with regard to the relevant biological role of pyrimidine antibacterials in the body [48]. Fig. 11 illustrates the spectral changes occurred in 1×10^{-4} M methanolic solution of $[Cu(Cl)_2(TMP)]$ upon addition of increasing amounts of CT DNA. Even though no appreciable change in the position of the intraligand band of metal complexes have been observed by addition of CT-DNA, the intensity of the band centered at 274 nm for $[Cu(Cl)_2(TMP)]$ (from 270 to 261 for $[Zn(Cl)_2(TMP)]\cdot(H_2O)$, from 296 to 272 for $[Pt(Cl)_2(TMP)]\cdot 3(H_2O)$, from 264 to 251 for $[Fe(Cl)_3(TMP)(H_2O)]$ and from 252 to 240 for $[Ru(Cl)_3(TMP)(H_2O)]\cdot(H_2O)$) complex has been increased in the presence of DNA up to $r = 9$ and a blue shift of 15 nm (259 nm) has been observed for higher amounts of DNA. The hypsochromic effect has been observed might be ascribed to external contact (electrostatic binding) [27,29] or that all complexes could uncoil the helix structure of DNA and made more bases embedding in DNA exposed [46–48]. The intrinsic binding constant K_b of $[Cu(Cl)_2(TMP)]$, $[Zn(Cl)_2(TMP)]\cdot(H_2O)$, $[Pt(Cl)_2(TMP)]\cdot 3(H_2O)$, $[Fe(Cl)_3(TMP)(H_2O)]$ and $[Ru(Cl)_3(TMP)(H_2O)]\cdot(H_2O)$ complexes with CT DNA represents the binding constant per DNA base pair, can be obtained by monitoring the changes in absorbances between 296 and 240 nm with increasing concentrations of CT DNA from plots $[DNA]/\varepsilon_a - \varepsilon_f$ versus [DNA] and is given by the ratio of slope to the y intercept, according to the following equation [47]:

$$\frac{[DNA]}{\varepsilon_a - \varepsilon_f} = \frac{[DNA]}{\varepsilon_b - \varepsilon_f} + \frac{1}{K_b(\varepsilon_b - \varepsilon_f)}$$

where $\varepsilon_a = A_{obsd}/[Complex]$, ε_f = extinction coefficient for the free complex and ε_b = extinction coefficient for $[Cu(Cl)_2(TMP)]$, $[Zn(Cl)_2(TMP)]\cdot(H_2O)$, $[Pt(Cl)_2(TMP)]\cdot 3(H_2O)$, $[Fe(Cl)_3(TMP)(H_2O)]$ and $[Ru(Cl)_3(TMP)(H_2O)]\cdot(H_2O)$ in the fully bound form. The high value of K_b obtained for $[Cu(Cl)_2(TMP)]$, $[Pt(Cl)_2(TMP)]\cdot 3(H_2O)$, $[Ru(Cl)_3(TMP)(H_2O)]\cdot(H_2O)$, $[Zn(Cl)_2(TMP)]\cdot(H_2O)$ and $[Fe(Cl)_3(TMP)(H_2O)]$, respectively, suggest a strong binding of complexes to CT DNA (Table 5). Indeed, it is much higher than K_b calculated for TMP ($=1.\pm 0.02 \times 10^3\ M^{-1}$), indicating that the coordination of TMP ligand to M(II)/(III) ion enhance significantly the ability to bind to CT DNA. This is an important point K_b of $[Cu(Cl)_2(TMP)]$, $[Pt(Cl)_2(TMP)]\cdot 3(H_2O)$, $[Ru(Cl)_3(TMP)(H_2O)]\cdot(H_2O)$, $[Zn(Cl)_2(TMP)]\cdot(H_2O)$ and $[Fe(Cl)_3(TMP)(H_2O)]$ is higher than the EB binding affinity for DNA ($K_b = 1.23 \pm 0.07 \times 10^5$) suggesting that electrostatic and

Table 5
The intrinsic binding constants (K_b) of complexes with CT DNA.

Complexes	K_b (±0.03)
TMP	2.50×10^4
$[Cu(Cl)_2(TMP)]$	6.66×10^7
$[Pt(Cl)_2(TMP)]\cdot 3(H_2O)$	6.57×10^7
$[Ru(Cl)_3(TMP)(H_2O)]\cdot(H_2O)$	6.48×10^7
$[Zn(Cl)_2(TMP)]\cdot(H_2O)$	6.25×10^7
$[Fe(Cl)_3(TMP)(H_2O)]$	6.14×10^7

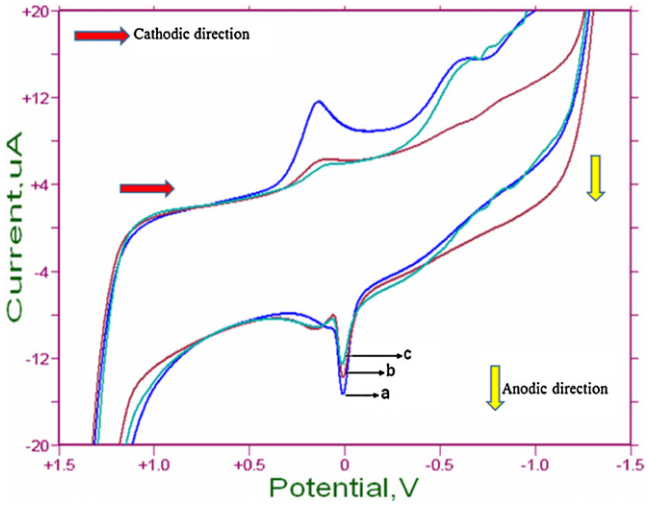

Fig. 12. The cyclic voltammograms of the $[Cu(Cl)_2(TMP)]$ complex in the presence of CT DNA in diverse r values. (a) 3×10^{-4} M $[Cu(Cl)_2(TMP)]$, (b) 100 μL DNA, and (c) 500 μLDNA. Initial potential: 1500 mV, high potential: 1500 mV, low potential: −1500 mV, scan rate: 100 mV/s, sensitivity: 10 μA/V, and number of the segments: 2.

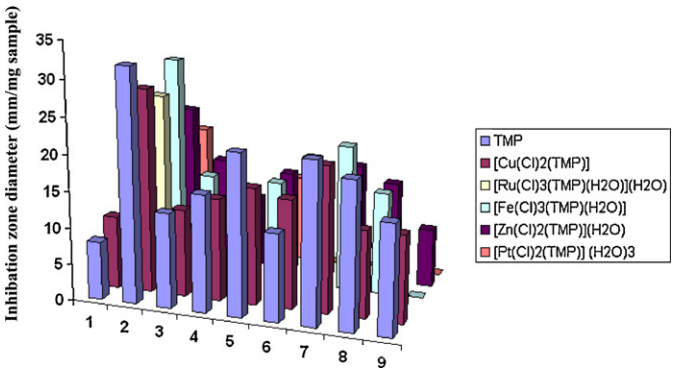

Fig. 13. Biological diagram of TMP and metal complexes, 1: *Candida albicans*, 2: *Saccharomyces cerevicia*, 3: *Eschericha coli*, 4: *Enterobacter cloaca*, 5: *Bacillus megaterium*, 6: *Bacillus cereus*, 7: *Pseudomonas* sp, 8: *Brusella melitensis*, and 9: *Staphylococcus aureus*.

intercalative interaction may affect EB displacement [49]. Also, the K_b value of free TMP has been found 2.5×10^4. This value is too smaller than the complexes K_bs values. This result clearly shows the importance of complexation.

The electrochemical investigations of metal–DNA interactions can provide a useful complement to spectroscopic methods, e.g., for nonabsorbing species, and yield information about interactions with both the reduced and oxidized form of the metal [50]. In Fig. 12, the cyclic voltammograms of the $[Cu(Cl)_2(TMP)]$ in the absence and presence of CT DNA, respectively, in diverse r values in Tris–HCl (pH 7) buffer solution are shown. It has been pointed out that the electrochemical potential of a small molecule will shift positively when it intercalates into DNA double helix, and if it is bound to DNA by electrostatic interaction, the potential would shift in a negative direction [29,51]. Additionally, in the case of more potentials than one, a positive shift of E_{p1} and a negative shift of E_{p2} imply that the molecule can bind to DNA by both intercalation and electrostatic interaction [20,52–54]. The quasi-reversible redox couple for each complex in 1/9 methanol/buffer solution that has been studied upon addition of CT-DNA and the shifts of the cathodic E_{pc} and anodic E_{pa} potentials are given in Table 6. Any new redox peaks have been appeared after the addition of CT DNA to each complex, but the current intensity of all the peaks have been increased significantly, suggesting the existence of an interaction between each complex and CT DNA. The increase in current intensity can be explained in terms of an equilibrium mixture of free and DNA-bound complex to the electrode surface [52]. It can be observed that complex for $[Cu(Cl)_2(TMP)]$ exhibits the same electrochemical behavior upon addition of CT DNA at diverse r values. For increasing amounts of CT DNA, the anodic potential E_{pa1} does not change after DNA binding but the cathodic potential E_{pc1} shows a negative shift ($\Delta E_{pc} = -15$ mV for $[Cu(Cl)_2(TMP)]$, while the anodic potential E_{pa2} shift to more positive values ($\Delta E_{pa} = +56$ mV for $[Cu(Cl)_2(TMP)]$. These shifts of the potentials show that all complexes can bind to DNA by both intercalation and electrostatic interaction [54]. A positive shift of the cathodic potential ($\Delta E_{pc2} = +10$ mV) of complex ($[Cu(Cl)_2(TMP)]$) has been observed while the first anodic potential remains unchanged (Fig. 13) followed by a slight increase of current intensity. The existence of intercalation between complex ($[Cu(Cl)_2(TMP)]$) and CT DNA bases can be suggested [27,50]. The conclusion derived from the CV study is that complexes $[Cu(Cl)_2(TMP)]$, $[Pt(Cl)_2(TMP)]\cdot 3(H_2O)$, $[Ru(Cl)_3(TMP)(H_2O)]\cdot(H_2O)$, $[Zn(Cl)_2(TMP)]\cdot(H_2O)$ and $[Fe(Cl)_3(TMP)(H_2O)]$ can bind to DNA by both intercalation and electrostatic interaction. Besides, the $E_{1/2}$ values of all complexes have been decreased after DNA addition.

The susceptibility of certain strains of bacterium towards TMP and its complexes has been judged by measuring the size of inhibition zone diameter. Antibacterial activities of TMP and its complexes have been carried out with three Gram-positive (*Bacillus megaterium*, *Bacillus cereus*, *Staphylococcus aureus*) and four Gram-negative (*Eschericha coli*, *Enterobacter cloaca*, *Pseudomonas* sp., *Brusellamelitensis*) bacteria. And antifungal screenings have been tested against two fungi (*Candida albicans*, *Saccharomyces cerevicia*). The test solutions have been prepared in DMSO. The results of the biological activities are summarized in Fig. 13. The synthesized compounds have been found to have remarkable bactericidal and fungicidal properties. Surprisingly $[Cu(Cl)_2(TMP)]$ and $[Zn(Cl)_2(TMP)]\cdot(H_2O)$ complexes show excellent activity against all type of bacteria and fungi. But, $[Ru(Cl)_3(TMP)(H_2O)]\cdot(H_2O)$ complex show activity only against *Saccharomyces cerevicia* fungi.

Such an increased activity of the metal chelates as compared to the TMP can be explained on the basis of chelation theory [53]. Chelation considerably reduces the polarity of the metal ion because of the partial sharing of its positive charge with the donor groups and possible p-electron delocalization over the chelate ring. Such chelation increases the lipophilic character of the central metal ion, which subsequently favors the permeation through the lipid layer of cell membrane. It is likely that the increased liposolubility of the ligand up on metal chelation may contribute to its facile transport into the bacterial cell which blocks the metal binding sides in enzyme of microorganisms [54,55].

Fig. 14a–h presents the scanning electron microscopic (SEM) images of the free PGE (a), activated PGE (b), CT DNA immobilized onto PGE (c), TMP on CT DNA immobilized onto PGE (d), $[Cu(TMP)Cl_2]$ on CT DNA immobilized onto PGE (e), $[Pt(Cl)_2(TMP)]\cdot 3(H_2O)$ CT DNA immobilized onto PGE (f), Cu(II) ions on CT DNA immobilized onto PGE (g) and Pt(II) ions on CT DNA immobilized onto PGE (h). The surface of the activated PGE (Fig. 14b) is smoother than the surface of the free PGE (Fig. 14a). When DNA is immobilized onto the surface of PGE (Fig. 14c), it has been seen that the surface of PGE changes and some plats occurs on the surface [56,57]. The SEM image of the TMP on CT DNA immobilized onto PGE has been shown in Fig. 14d. The effective change on the surface and increase of the plats shows the interaction between TMP and DNA. SEM photographs of the synthesized copper and platinum complexes of TMP on CT DNA are illustrated in Fig. 14e and f, respectively. The $[Pt(Cl)_2(TMP)]\cdot 3(H_2O)$

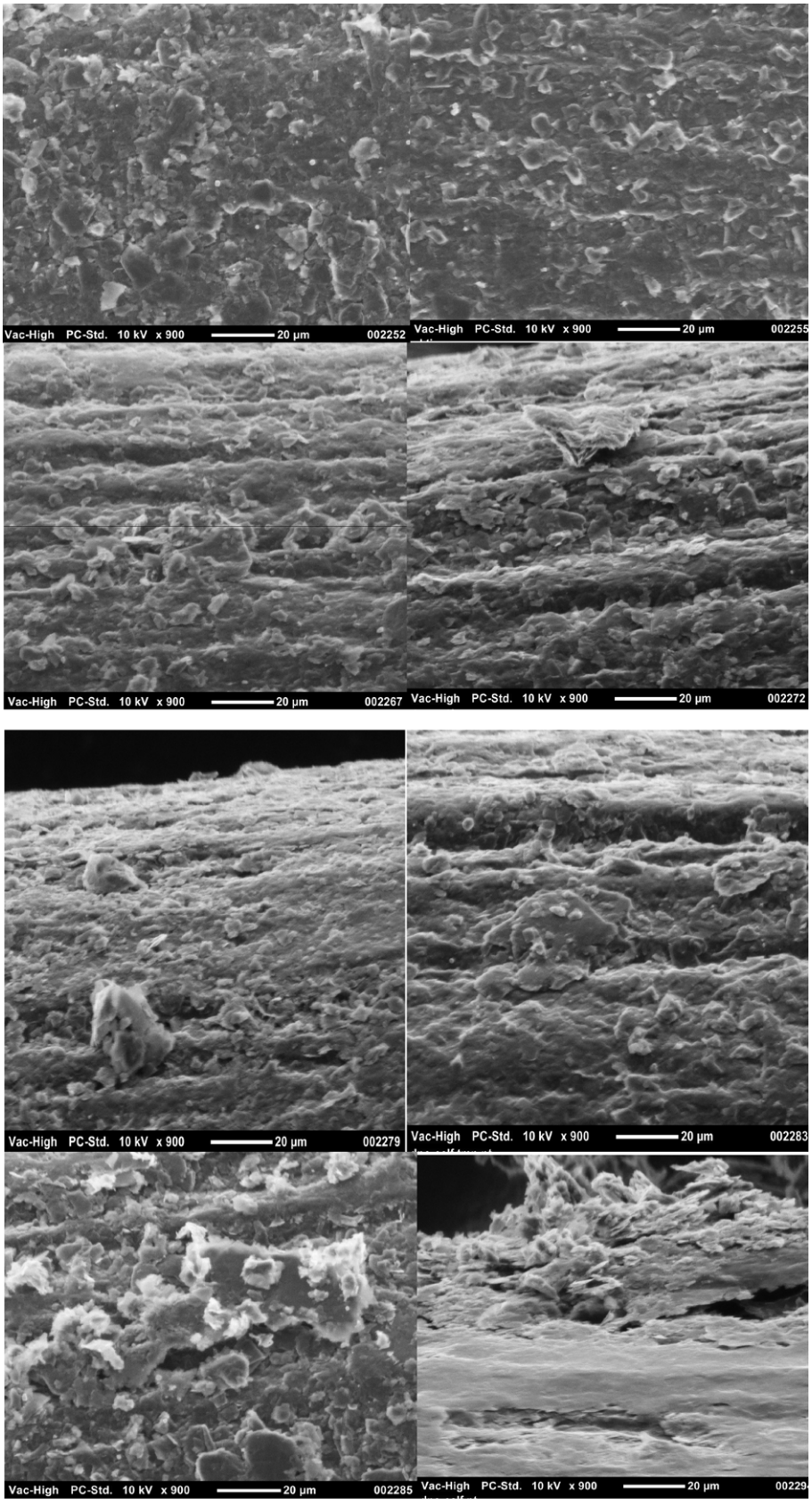

Fig. 14. The SEM images of free PGE (a), activated PGE (b), CT DNA immobilized onto PGE (c), TMP CT DNA immobilized onto PGE (d), $[Cu(TMP)Cl_2]$ CT DNA immobilized onto PGE (e), $[Pt(Cl)_2(TMP)]\cdot 3(H_2O)$ CT DNA immobilized onto PGE (f), Cu(II) ions on CT DNA immobilized onto PGE (g) and Pt(II) ions CT DNA immobilized onto PGE (h).

Table 6
Cathodic and anodic potentials and the shift of the potentials in the absence and presence of CT-DNA of [$Cu(Cl)_2$TMP] complex.

Complex	Redox couple	E_{pc1} [f]	E_{pa1} [f]	ΔE_1 [f]	$(E_{1/2}{}^f)_1$	E_{pc2} [f]	E_{pa2} [f]	ΔE_2 [f]	$(E_{1/2}{}^f)_2$
[$Cu(Cl)_2$TMP]	Cu(II)/Cu	+143	+8	−135	75.5	−603	+98	+701	−252.5
Complex	E_{pc1} [b]	E_{pa1} [b]	ΔE_1 [b]	$(E_{1/2}{}^b)_1$	E_{pc2} [b]	E_{pa2} [b]	ΔE_2 [b]	$(E_{1/2}{}^b)_2$	
[$Cu(Cl)_2$TMP]	+128	+6	−122	+67	−593	+154	+747	−142.5	

$\Delta E = E_{pa} - E_{pc}$; $E_{1/2} = 1/2 \times (E_{pa} + E_{pc})$.

complex CT DNA immobilized onto PGE has changed the surface much more than the [$Cu(TMP)Cl_2$] complex CT DNA immobilized onto PGE. In addition to all of these data, it has been recorded that SEM images of Cu(II) ions on CT DNA immobilized onto PGE (Fig. 14g) and Pt(II) ions on CT DNA immobilized onto PGE (Fig. 14h). Similar to platinum complex, the platinum(II) ions have caused big changes on the surface respectively to copper(II) ions.

This immobilization on the surface has also been recorded as voltammetric signal [38,57]. The optimization of the immobilization step of CT DNA on the PGE is shown in Fig. 15a as voltammetric signal. The guanine oxidation peak has been used as an indicator. Different concentrations of CT DNA have been immobilized and the maximum surface coverage the PGE has been obtained before interaction with TMP (or metal ions or metal complexes) by DPV technique. The guanine has been oxidized at about +1.02 V. For finding the optimum concentration of CT DNA, five different concentrations between 1 and 10.00 ppm have been studied. During this step, CT DNA has been immobilized at +0.5 V. Guanine peak current has been increased with increasing CT DNA concentration to 4 ppm and then leveled off. The effects of the experimental parameters have been studied to find optimum analytical conditions for interaction between TMP and CT DNA (Fig. 15b). The binding of the TMP to the CT DNA modified PGE has been optimized depending on the interaction concentration by DPV in Tris–HCl buffer solution containing 30% ethanol. After the interaction with TMP, the guanine signal has been decreased linearly. In this way, different TMP concentrations have been studied between 0.00 and 12.00 ppm as seen in Fig. 15b. The best results have been obtained at 10.00 g/mL TMP concentration. Similar calibration studies have been done for [$Cu(TMP)Cl_2$] complex and the results have been given in Fig. 15c. According to voltammetric results, voltammetric signal of TMP CT DNA immobilized onto PGE is greater than the[$Cu(TMP)Cl_2$] complex CT DNA immobilized onto PGE (Fig. 15d).

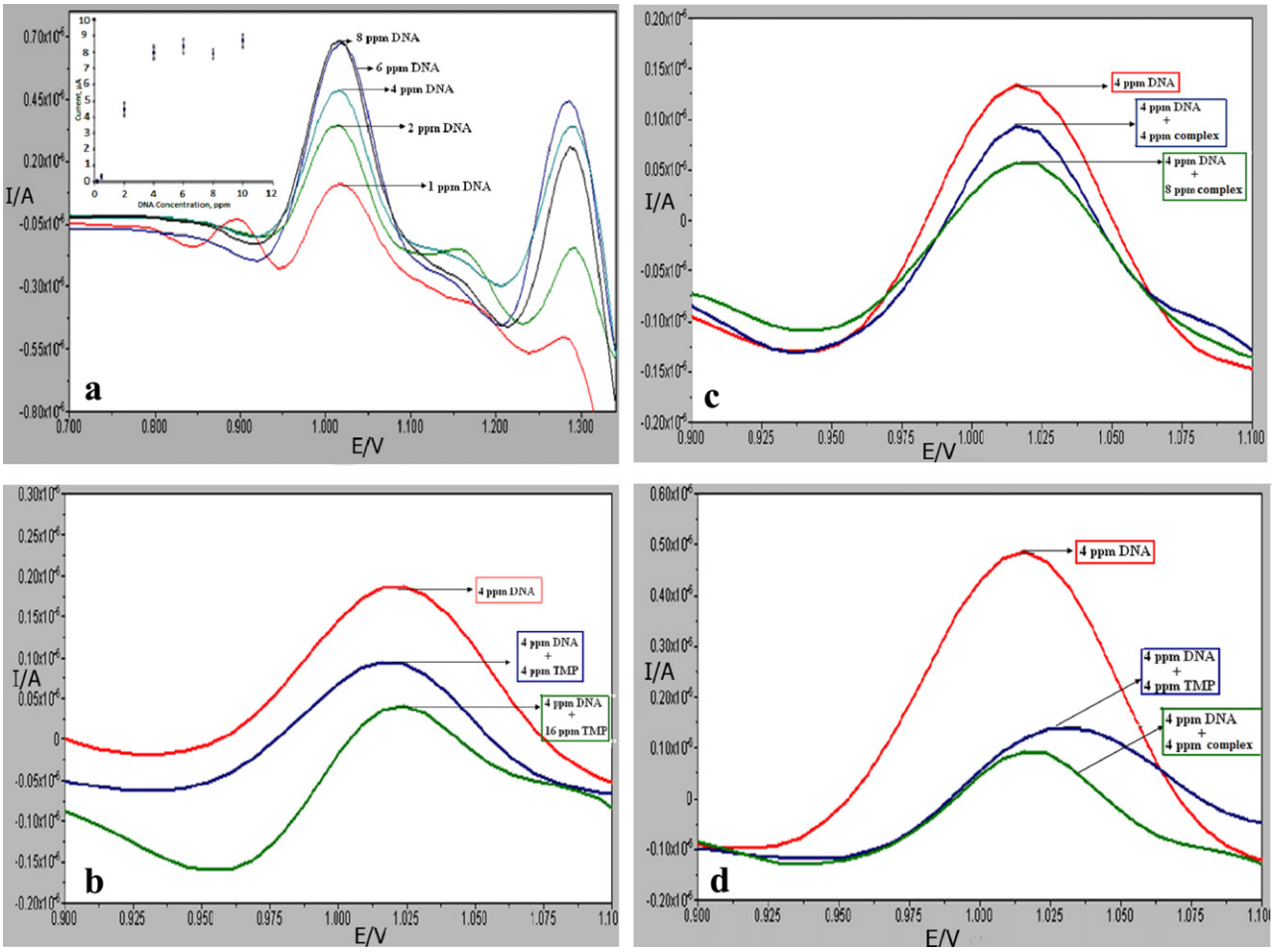

Fig. 15. The effect of CT DNA concentration at oxidation signal at PGE for the optimization of immobilization of dsDNA (a). DP voltammograms for the interaction of 4 ppm CT DNA modified PGE with several concentrations of TMP (b). DP voltammograms for the interaction of 4 ppm CT DNA modified PGE with several concentrations of [Cu(TMP)Cl2] complex (c). DP voltammograms for the interaction of 4 ppm CT DNA modified PGE with 4 ppm TMP and 4 ppm [Cu(TMP)Cl2] complex (d).

4. Conclusion

The synthesis and characterization of five new TMP to complexes with Cu(II), Pt(II), Zn(II), Fe(III) and Ru(III) have been synthesized with physicochemical and spectroscopic methods. The study of the complexes interaction with CT DNA has been performed with UV spectroscopy and cyclic voltammetry and it reveals that the complexes can bind to DNA. UV spectroscopic titrations have been used in order to calculate the binding strength of the complexes with CT DNA which is mirrored in the intrinsic binding constant K_b [Cu(TMP)Cl_2] complex exhibits much higher intrinsic binding constant to CT DNA than the other complexes. The results have been described in this study show that changing the metal environment can modulate the binding property of the complex with DNA [42]. Information obtained from the present is helpful to the development of nucleic acids molecular probes and therapeutic agents. In addition, it would be of considerable interest if the novel DNA adducts of [Cu(TMP)Cl_2] complex led to a broader spectrum of antibacterial activity. Cyclic voltammetric studies have shown that all complexes bind to CT DNA by both intercalation and electrostatic interaction. The most of bacterial infections now defy all known antibiotics and the antibiotic resistance is a growing problem in our environment. There is a great need for new antibacterial agents and metal complexes as novel derivatives of pyrimidines can play an important role in this field. In most cases, it has been evidenced that the antimicrobial activity of the complexes is comparable to free pyrimidine. According to our biological results, because of the chelate effect, some complexes ([$Cu(Cl)_2$(TMP)], [$Fe(Cl)_3$(TMP)(H_2O)] and [$Zn(Cl)_2$(TMP)]·(H_2O)) exhibited higher inhibitory activity than TMP against some microorganisms.

The investigation of drug–CT DNA interactions would provide new compounds to be tested for an effect on a biochemical target, for the design of DNA biosensors, which will further become DNA microchip systems [56]. In this paper, the interaction between antibacterial drug TMP and its Cu(II), Zn(II), Pt(II), Fe(III), Ru(III) and CT DNA has been investigated by voltammetry and spectrophotometry for the first time. An electrochemical CT DNA biosensor has been prepared by immobilizing CT DNA onto PGE surface. The oxidation signal of guanine has been used as probe for the investigation of the interaction between compounds and CT DNA. As a result of the interaction of compounds in different concentrations with CT DNA, a decrease has been observed in the response based on the signal of guanine. This phenomenon can be explained by the damage on the oxidizable group of electroactive base guanine because of the diffusion of compounds [57]. Also, interaction of CT DNA in different concentrations with compounds, positive/negative peak potentials shift may indicate that the compound binding to DNA by both intercalation and electrostatic interaction. It is clear that, the results of spectrophotometry and voltammetry used glassy carbon electrode are in accordance with the results of voltammetry used PGE. The utility of this electrochemical biosensor for the interaction between CT DNA and compounds are cost effective and it provides rapid detection.

Acknowledgments

The authors wish to thank TUBITAK (Project No.: 109T020), KSU (Project No.: 2009/4-12 and Project No.: 2010/5-19) for the financial supports and Prof. Dr. Metin Dıgrak (Department of Biology, Faculty of Science and Letters, University of Kahramanmaras Sutcu Imam, Campuse of Avsar, 46100 Kahramanmaras, Turkey) for antimicrobial studies.

References

[1] L. Rajith, K.G. Kumar, Drug Test. Anal. 2 (2010) 436–441.
[2] P.J. Sadler, Adv. Inorg. Chem. 36 (1991) 1–48.
[3] N. Saha, S. Kar, J. Inorg. Nucl. Chem. 39 (1977) 195–200.
[4] D. Kovala, N. Hadjiliadis, J. Tsangaris, J. Less Common Met. 115 (1986) 1–5.
[5] J. Tsangaris, D. Sotiropoulos, A. Galinos, Inorg. Nucl. Chem. Lett. 14 (1978) 445–449.
[6] F. Demartin, M. Manassero, L. Naldini, M. Zoroddu, Inorg. Chim. Acta 213 (1983) L213–L214.
[7] L. Naldini, M. Cabras, M. Zoroddu, F. Demartin, M. Manassero, M. Sansoni, Inorg. Chim. Acta 88 (1984) 45–50.
[8] M. Zoroddu, L. Naldini, F. Demartin, N. Masciocchi, Inorg. Chim. Acta 128 (1987) 179–183.
[9] F. Demartin, N. Masciocchi, L. Naldini, A. Panzanelli, M. Zoroddu, Inorg. Chim. Acta 171 (1990) 229–233.
[10] P.T. Muthiah, J.J. Robert, J. Chem. Crystallogr. 29 (1999) 223–226.
[11] U. Habib, A. Badshah, U. Flörke, R.A. Qureshi, B. Mirza, N. Islam, A. Khan, J. Chem. Crystallogr. 39 (2009) 730–734.
[12] U. Habib, A. Badshah, U. Flörke, R.A. Qureshi, B. Mirza, N. Islam, A. Khan, J. Chem. Crystallogr. 39 (2009) 607–611.
[13] B. Simo, L. Perello, R. Ortiz, A. Castineiras, J. Latorre, E. Canton, J. Inorg. Biochem. 81 (2000) 275–283.
[14] B. Seekhon, H. Randhawa, H. Sahai, Synth. React. Inorg. Met.-Org. Chem. 29 (1999) 309–321.
[15] J.E. Weder, C.T. Dillon, T.W. Hambley, B.J. Kennedy, P.A. Lay, J.R. Biffin, H.L. Regtop, N.M. Davis, Coord. Chem. Rev. 232 (2002) 95–126.
[16] P.A. Ajibade, G.A. Kolawole, Transit. Met. Chem. 33 (2008) 493–497.
[17] M.J. Clarke, Coord. Chem. Rev. 236 (2003) 207–231.
[18] P.A. Ajibade, G.A. Kolawole, Synth. React. Inorg. Met.-Org. Chem. 40 (2010) 273–278.
[19] P.A. Ajibade, G.A. Kolawole, J. Coord. Chem. 61 (2008) 3367–3374.
[20] P.A. Ajibade, G.A. Kolawole, P. O'Brien, J. Coord. Chem. 61 (2008) 328–340.
[21] M.V. Lokhande, Asian J. Chem. 18 (2006) 2662–2668.
[22] P.A. Ajibade, G.A. Kolawole, P. O'Brien, J. Coord. Chem. 59 (2006) 1621–1628.
[23] G. Karthikeyan, K.M. Raj, K.R. Elango, K.G. Kumar, J. Chem. Res. S (2004) 200–202.
[24] B.S. Sekhon, H.K. Sahai, H.S. Randhawa, Natl. Acad. Sci. Lett. 21 (1998) 76–78.
[25] F. Demartin, M. Manassero, L. Naldini, M.A. Zoroddu, Inorg. Chim. A: Art. Lett. 77 (1983) L213–L214.
[26] L. Naldini, M.A. Cabras, M.A. Zoroddu, F. Demartin, M. Manassero, M. Sansoni, Inorg. Chim. A: Art. Lett. 88 (1984) 45–50.
[27] G. Psomas, J. Inorg. Biochem. 102 (2008) 1798–1811.
[28] Q. Xin, M. Zhong-Ying, X. Cheng-Zhi, X. Fei, Z. Yan-Wen, X. Jing-Yuan, Q. Zhao-Yan, L. Jian-Shi, C. Gong-Jun, Y. Shi-Ping, J. Inorg. Biochem. 105 (2011) 728–737.
[29] M. Carter, A.J. Bard, M. Rodriguez, J. Am. Chem. Soc. 111 (1989) 8901–8911.
[30] S. Dey, S. Sarkar, T. Mukherjee, B. Mondal, E. Zangrando, J.P. Sutter, P. Chattopadhyay, Inorg. Chim. Acta 376 (2011) 129–135.
[31] J. Wang, Anal. Chim. Acta 469 (2002) 63–71.
[32] E. Paleček, Electroanalysis 21 (2009) 239–251.
[33] Y. Yardim, E. Keskin, A. Levent, M. Ozsoz, Z. Senturk, Talanta 80 (2010) 1347–1355.
[34] M.A.B. Christopher, O.B. Ana Maria, H.P.S. Silvia, J. Electroanal. Chem. 366 (1994) 225–231.
[35] S.K. Shankara, J. Seetharamappa, S.N. Prashanth, Colloids Surf. B 82 (2011) 438–442.
[36] C.H. Collins, P.M. Lyne, J.M. Grange, Microbiological Methods, Butterworths & Co. Ltd., London, 1989, pp. 103–115.
[37] J. Wang, A.N. Kawde, E. Sahlin, Analyst 125 (2000) 5–7.
[38] B. Dogan-Topal, B. Uslu, S.A. Ozkan, Biosens. Bioelectron. 24 (2009) 2358–2364.
[39] M. Dolaz, V. McKee, S. Urus, N. Demir, A.E. Sabik, A. Golcu, M. Tumer, Spectrochim. Acta A 76 (2010) 174–181.
[40] S.E. Castillo-Blum, N. Barba-Behrens, Coord. Chem. Rev. 196 (2000) 3–30.
[41] H. Muslu, A. Golcu, M. Tumer, M. Ozsoz, J. Coord. Chem. 64 (2011) 3393–3407.
[42] M. Kotoucek, J. Skopalova, D. Michalkova, Anal. Chim. Acta 353 (1997) 61–69.
[43] A. Golcu, B. Dogan, S. Ozkan, Talanta 67 (2005) 703–712.
[44] D. Tarinc, B. Dogan-Topal, M. Dolaz, A. Golcu, S.A. Ozkan, Curr. Anal. Chem. 6 (2010) 316–328.
[45] H. Muslu, A. Golcu, S.A. Ozkan, Curr. Anal. Chem. 6 (2010) 299–309.
[46] T.M. Kelly, A.B. Tossi, D.J. McConnel, T.C. Strekas, Nucleic Acids Res. 13 (1985) 6017–6034.
[47] A.M. Pyle, J.P. Rehmann, R. Meshoyrer, C.V. Kumar, N.J. Turro, J.K. Barton, J. Am. Chem. Soc. 111 (1989) 3053–3063.
[48] H. Chao, W.-J. Mei, Q.-W. Huang, L.-N. Ji, J. Inorg. Biochem. 92 (2002) 165–170.
[49] A. Dimitrakopoulou, C. Dendrinou-Samara, A.A. Pantazaki, M. Alexiou, E. Nordlander, D.P. Kessissoglou, J. Inorg. Biochem. 102 (2008) 618–628.
[50] M.T. Carter, A.J. Bard, J. Am. Chem. Soc. 109 (1987) 7528–7530.
[51] S.-S. Zhang, S.-Y. Niu, B. Qu, G.-F. Jie, H. Xu, C.-F. Ding, J. Inorg. Biochem. 99 (2005) 2340–2347.
[52] S. Tabassum, S. Parveen, F. Arjmand, Acta Biomater. 1 (2005) 677–689.
[53] S.K. Mandal, K. Nag, J. Chem. Soc. Dalton Trans. 11 (1983) 2429–2434.
[54] E. Chartone-Souza, T.L. Loyola, M.B. Rodriguez, M.-A. de, B.C. Menezes, N.A. Rey, E.C. Pereira-Maia, J. Inorg. Biochem. 99 (2005) 1001–1008.
[55] A.S. Gordon, L.D. Howell, V. Harwood, Can. J. Microbiol. 40 (1994) 408–411.
[56] A. Erdem, M. Ozsoz, Electroanalysis 14 (2002) 965.
[57] L.L. Wu, J.Z. Zhou, J. Luo, Electrochim. Acta 45 (2000) 2923.